Synthesis, Characterization, and Photocatalytic Activities of Nanoparticulate N, S-Codoped TiO_2 Having Different Surface-to-Volume Ratios

Julian A. Rengifo-Herrera,[†,‡] Katarzyna Pierzchała,[§] Andrzej Sienkiewicz,[§] Laszlo Forró,[§] John Kiwi,[†] Jacques E. Moser,[‡] and Cesar Pulgarin*[,†]

SB, ISIC, GGEC, station 6, SB, ISIC, GR-MO, station 6, and SB, IPMC, LNNME, station 3, Ecole Polytechnique Fédérale de Lausanne, 1015, Lausanne, Switzerland

Received: November 3, 2009; Revised Manuscript Received: December 29, 2009

An efficient, visible light active, N, S-codoped TiO_2-based photocatalyst was prepared by reacting thiourea with nanoparticulate anatase TiO_2. Commercial anatase powders were manually ground with thiourea and annealed at 400 °C in two crucibles with different surface-to-volume ratios ($S/V = 20$ and 1.5) to prepare two N, S-codoped TiO_2 materials. The differentiated aeration conditions during the catalyst annealing on the crucibles allowed for different amounts of O_2 to reach the catalyst surface. The first material, with $S/V = 20$, herein referred to as D-TKP 102-A, was clear beige colored. The second material, with $S/V = 1.5$, herein referred to as D-TKP 102-B, was darker and revealed a markedly lower efficiency in *Escherichia coli* inactivation. The D-TKP 102-A powder presented visible light absorption due to the nitrogen (N) and sulfur (S) doping. X-ray photoelectron spectroscopy signals for this catalyst were observed for N 1s peaks at binding energies of 399.2 and 400.7 eV due to interstitial N-doping or Ti−O−N species. The S 2p were due to SO_4^{-2} signals with BE > 168 eV and signals at 162.8 and 167.2 eV due to anionic and cationic S-doping, respectively. By fast kinetic spectroscopy, the decay of the electron induced by pulsed light at $\lambda = 450$ nm (∼8 ns/laser pulse) was followed for the D-TKP 102-A catalyst. Undoped D-TKP 102 catalyst did not promote the electron in the visible range, and consequently no signal decay could be observed in the latter case. Low-temperature electron spin resonance measurements at 8 K provided evidence for electrons trapped in shallow traps, such as oxygen vacancies, V_o, induced by N, S doped on D-TKP 102-A. The ESR measurements implementing the reactive scavenging with singlet oxygen scavenger, TMP−OH, revealed the production of singlet oxygen ($^1O_2$).

1. Introduction

Heterogeneous photocatalysis, a promising technology in environmental cleanup, is mostly based on the semiconductor photocatalyst nanocrystalline titanium dioxide (TiO_2).[1,2] In particular, anatase-type TiO_2 shows high photocatalytic activities and has already found numerous applications in the removal of pollutants from air and water.[1,2] However, an important drawback of TiO_2 for applications in photocatalysis is that its band gap is rather large (3.0−3.2 eV). Thus, the overall photocatalytic efficiency of TiO_2 is limited to only a small fraction of the solar spectrum corresponding to the UV region ($\lambda < 387$ nm), which accounts for ∼4% of the incident solar energy. In recent years, shifting of the absorption spectrum of TiO_2 from the UV region into the visible light range has attracted much attention.[3,4] In particular, over the past decade, much progress has been achieved in the field of preparing TiO_2-based formulations absorbing in the main part of the solar spectrum. Visible light-activated TiO_2 can be prepared by several methods, including metal-ion implantation, reducing of TiO_2, sensitizing of TiO_2 with dyes, or nonmetal doping by incorporation of various dopants into the TiO_2 lattice.[5,6] In the case of nonmetal doping of TiO_2, incorporation of such nonmetals as N or S by different ways has been used the most frequently.[7] In particular, depending on the preparation method it has been possible to obtain N- or S-doped TiO_2 with interstitial or substitutional N-doping,[8,9] leading to materials with different photocatalytic activities.[10] Several preparation methods have been recently reported by Livraghi et al.[11] for N-doped TiO_2. This study reports on the dependence of the visible light absorption and the photocatalytic activity of N-doped TiO_2 upon the nature of N-doping (substitutional or interstitial). In this context, Fu et al.[12] have suggested the possibility of ·OH radicals formation by N-doped TiO_2 under visible light. Recent studies have shown that the visible light-induced electron promoted to the conduction band might be responsible for the photocatalytic activity on N-TiO_2.[13−15] In our recent study on N, S-codoped TiO_2, we have found evidence that photoexcited electrons promoted by visible light irradiation could participate in redox reactions on the semiconductor surface, leading to the formation of superoxide radical ($\cdot O_2^-$) and singlet oxygen ($^1O_2$).[16]

In this study, we report on preparation, characterization, and photocatalytic activity toward *Escherichia coli* (*E. coli*) photoinactivation of two N, S-codoped TiO_2 materials annealed in two crucibles having different surface−volume (*S*/*V*) ratios. The characterization of these materials was performed using various spectroscopic techniques, including diffuse reflectance spectroscopy, X-ray photoelectron spectroscopy, attenuated total reflectance infrared spectroscopy, low-temperature electron spin resonance (ESR), ESR spin-trapping, and diffuse reflectance time-resolved spectroscopy.

* To whom correspondence should be addressed. Tel.: +41 21 693 47 20. Fax: +41 21 693 6161. E-mail: cesar.pulgarin@epfl.ch.
† SB, ISIC, GGEC, station 6.
‡ SB, ISIC, GR-MO, station 6.
§ SB, IPMC, LNNME, station 3.

10.1021/jp910486f
Published on Web 01/25/2010

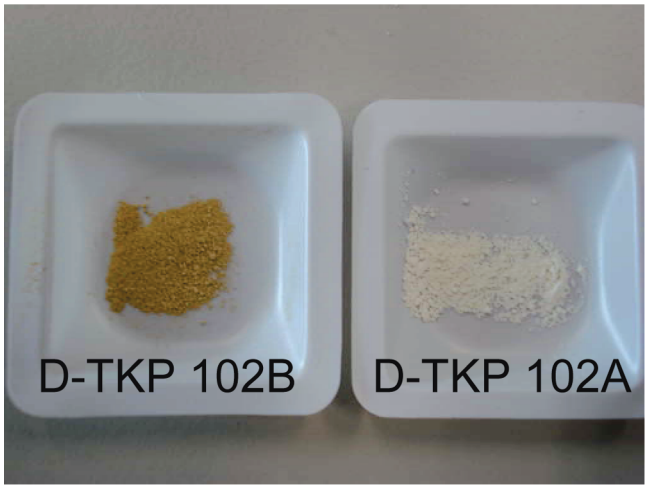

Figure 1. Photo of D-TKP 102-B and D-TKP 102-A powders obtained.

2. Experimental Section

2.1. Materials. Tayca Corporation kindly supplied commercial TiO_2, TKP 102 (96% anatase, primary crystallite particle size of 15 nm). Thiourea (99% Sigma-Aldrich) was used as received.

2.2. Preparation of Doped Tayca TKP 102. First, the commercial TiO_2 anatase, TKP-102, was manually mixed with thiourea in a 4:1 ratio. Subsequently, the mixed material was divided into two batches and annealed in ceramic crucibles having different dimensions, which allowed for differentiated aeration conditions for each of the batches. The annealing process was performed for 1 h at 400 °C under air atmosphere with the heating rate of 10 °C min^{-1}, which was then followed by cooling at room temperature. This allowed for different amounts of gaseous oxygen to reach the catalyst surface. Figure 1 shows the two obtained materials, D-TKP 102-A and D-TKP 102-B, having markedly different colors. The clear catalyst, D-TKP 102-A, was annealed in a crucible with dimensions $r = 6$ cm and $h = 0.1$ cm, whereas the dark catalyst, D-TKP 102-B, was annealed in a crucible with dimensions $r = 2.5$ cm and $h = 3$ cm. After annealing both materials were washed with Milli-Q water three times, dried at 70 °C, and crushed in an agate mortar into a fine powder.

2.3. Powder Characterization. ***2.3.1. Diffuse Reflectance Spectroscopy (DRS).*** DRS spectra of TiO_2 powders were measured with a Varian Cary 1E spectrophotometer equipped with a diffuse reflectance accessory.

2.3.2. X-ray Photoelectron Spectroscopy (XPS). XPS analyses were carried out on a XPS Analyzer Kratos model Axis Ultra with a monochromatic AlK_α and charge neutralizer. The deconvolution software program was also provided by Kratos. This software is the standard program used and is accepted as reference in the field. The binding energies (BE) were referenced to the 285 eV C1s peak of carbon. Powder samples were prepared by deposition of the catalyst on carbon-coated sample holder. The powder samples were analyzed in an oversized spot with dimension 0.3 × 0.7 mm to record a spectrum characteristic for "average" particles. Using a large spot also the signal/noise ratio was significantly improved, and concomitantly the accumulation time was increased since the signal/noise ratio was weak. This was not necessary for N since its sensitivity was not weak. The detection limit was not 0.1 at. % but 0.03 at. %.

Sputter profiling was performed by each sample with 3 keV Ar^+ ions at an angle of incidence (θ) of 45° to the normal to the sample. Etching time was around 120 s corresponding to a depth around 4 nm.

2.3.3. Attenuated Total Reflectance Fourier Transform Infrared Spectroscopy (ATR-FTIR). These measurements were carried out using a FT-IR spectrometer Perkin-Elmer equipped with an ATR accessory. Spectra were recorded using 1024 scans having a resolution of 4 cm^{-1}.

2.3.4. Diffuse Reflectance Time-Resolved Spectroscopy (DRTRS). N, S-codoped TKP 102 powders were positioned in a custom-built diffuse reflectance accessory and excited by nanosecond laser pulses produced by a Continuum Powerlite 7030 frequency-doubled Q-switched Nd:YAG laser (λ= 450 nm, 30 Hz repetition rate, pulse width at half-height of 8 ns, pulse fluence of 200*i*J cm^{-2}). The probe light from a Xe arc lamp was passed through a monochromator, sample, and a second monochromator before reaching the fast photomultiplier tube. Typically, averaging over 1000 laser shots was necessary to get an acceptable signal/noise level.

2.3.5. Low-Temperature Electronic Spin Resonance. Low-temperature continuous wave (cw) ESR measurements were carried out with a Bruker ESR spectrometer E500 EleXsys Series (Bruker Biospin GmbH) equipped with a Gunn diode-based microwave bridge (model SuperX), a Bruker ER 4122 SHQE cavity, and an Oxford Instruments helium-gas continuous flow cryostat (ESR900). The 100 kHz modulation amplitude was kept at 2 G (0.2 mT) to avoid modulation broadening.

2.3.6. ESR Spin Trapping of Radicals. *2.3.6.1. ESR Scavenging of Singlet Oxygen.* For the study of ESR reactive scavenging of singlet oxygen, 3.2 mg of N- and S-doped TiO_2 powder was suspended in 10 mL of either ultrapure H_2O or D_2O (99.9% atomic purity from Aldrich). The diamagnetic singlet oxygen-scavenging reagent, 2,2,6,6-tetramethyl-4-piperidinol (TMP−OH), from Fluka was used as received to detect singlet oxygen formation in the aqueous (H_2O and D_2O) suspensions of N- and S-doped TiO_2. TMP−OH reacts with singlet oxygen yielding a paramagnetic product, 4-hydroxy-2,2,6,6-tetramethylpiperidine-1-oxyl (TEMPOL). This technique, introduced by Lion et al.,[17] is specific for the detection of singlet oxygen.[18] The final concentration of TMP−OH was adjusted to 2.5 mM. One milliliter of suspension was transferred into a 5 mL Pyrex beaker and exposed to the light source (150 W halogen lamp, model 6000, Intralux, Switzerland). Samples were stirred during illumination.

2.3.6.2. ESR Detection of Spin-Trapped ROS and Reactively Scavenged Singlet Oxygen. Immediately after subsequent exposures to white light illuminations, aliquots of ca. 7 μL of illuminated suspensions were transferred into 0.7 mm i.d. and 0.87 mm o.d. quartz capillary tubes from VitroCom, NJ (sample height of 25 mm), and sealed on both ends with Cha-Seal™ tube sealing compound (Medex International, Inc., U.S.). ESR experiments were carried out at room temperature using an ESP300E spectrometer (Bruker BioSpin GmbH), equipped with a standard rectangular mode TE_{102} cavity. Routinely, for each experimental point, five-scan field-swept ESR spectra were recorded. The typical instrumental settings were microwave frequency 9.38 GHz, microwave power 2.0 mW, sweep width 120 G, modulation frequency 100 kHz, modulation amplitude 0.5 G, receiver gain 4×10^4, time constant 20.48 ms, conversion time 40.96 ms, and time per single scan 41.9 s.

2.4. Photocatalytic Activity. Cylindrical Pyrex reactors (50 mL) were used as photoreactors. A TiO_2 concentration of 1.0 g L^{-1} was suitable and selected after preliminary experiments were selected, and the oxygen of the air was the electron acceptor. The suspension was kept under magnetic stirring and illuminated

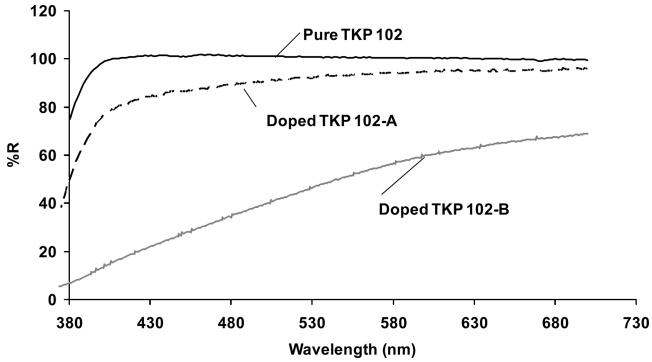

Figure 2. DRS spectra of doped and undoped TKP 102 powders.

by five fluorescent lamps Phillips TLD-18W blue (emission spectra, 400−500 nm; UV intensity, 0.1 W m^{-2}; and intensity between 290 and 1100 nm, 60 W m^{-2}). The radiant flux was monitored with a Kipp & Zonen (CM3) power meter (Omni instruments Ltd., Dundee, U.K.). The temperature of the experiments was never superior to 38 °C. Samples were periodically collected to follow the reaction kinetics. Results represent the average of three experimental runs, and their standard deviations were equal to or lower than 15% for the microbiological analysis.

Bactericidal inactivation was measured by sampling *E. coli* strain K12 (MG 1655) in the photoreactor at preset sampling times. Before the experiment, bacteria were inoculated into nutrient broth (Oxoid No. 2, Switzerland) and grown overnight at 37 °C. During the stationary growth phase, bacteria cells were harvested by centrifugation at 5000 rpm for 10 min at 4°C. The bacterial pellet was then washed three times with a saline solution (8 g L^{-1} NaCl and 0.8 g L^{-1} KCl in Milli-Q water, at pH 7 by addition of HCl or NaOH). A suitable cell concentration (10^4 colony forming units per milliliter (CFU mL^{-1})) was inoculated in the reactor's saline solution. Then, the inoculated Pyrex bottles with the catalyst added were illuminated for 2 h, and samples (1.0 mL) were taken at different time intervals. Serial dilutions were performed in saline solution, and 100 μL volumes were inoculated in a plate count agar (PCA, Merck, Germany) growth medium. The number of colonies was counted 24 h after inoculation at 37 °C. Control experiments involving *E. coli* and UV or visible light without catalyst and *E. coli* in the presence of catalyst in the dark were performed.

3. Results and Discussion

3.1. Visible Light Absorption of Doped TiO_2 Powders. Figure 2 shows the plot of the reflectance percent (*%R*) vs wavelength obtained from DRS measurements. Reflectance at 100% means no light absorption. Pure TKP 102 powder showed the characteristic anatase absorption at wavelengths <400 nm. Visible light absorption was observed for the powders annealed with thiourea, and the D-TKP 102-B powder showed a higher visible absorption than D-TKP 102-A.

3.2. Characterization by X-ray Photoelectron Spectroscopy (XPS). Figure 3 shows the XPS spectrum of D-TKP 102-B with N 1s peak at 396 eV due to Ti−N bonds or substitutional N-doping[7,19−21] and C 1s peaks at 281 and 284 eV. The peak at 284 eV is due to adventitious carbon. In contrast, the signal at 281 eV is due to Ti−C bonds[22,23] due probably to C-doped TiO_2. The S 2p spectrum did not reveal the presence of S 2p peaks linked to S-doping of TiO_2.

Figure 4 shows the high-resolution XPS spectra of D-TKP 102-A powder. XPS spectra revealed the presence of two N 1s peaks at binding energies (BE) of 399.2 and 400.7 eV assigned to interstitial N-doping (Ti−O−N species).[10,24] The S 2p peaks for sulfur are found for high oxidation states (such as SO_4^{-2}) at BE >168 eV. The additional sulfur peaks between 163 and 166 eV were due to the presence of SO_3^{2-} species.[25] The other two peaks related to S-doping were found at 162.8 and 167.2 eV and originate from anionic-S and cationic-S species, respectively.[26,27] C 1s peaks assigned to C−O and C═O bonds were found at binding energies around 286.6 and 288.6 eV, respectively.[28,29] Doped TKP 102-B showed a higher N concentration than doped TKP 102-A, while the S concentration was similar in both materials (see Table 1).

Ar^+ ion sputtering was carried out with an etching time at 120 s of the topmost layers (a depth around 4 nm), and the results are shown in Figures 3 and 5. For D-TKP 102-B powders (Figure 3), the N 1s peak was found at 396 eV, and C 1s peaks at 284 and 281 eV decreased in intensity due to etching. Ti 2p and O 1s peaks at 459, 465, and 530 eV, respectively, and linked to Ti−O bonds in TiO_2 increased their intensities during the

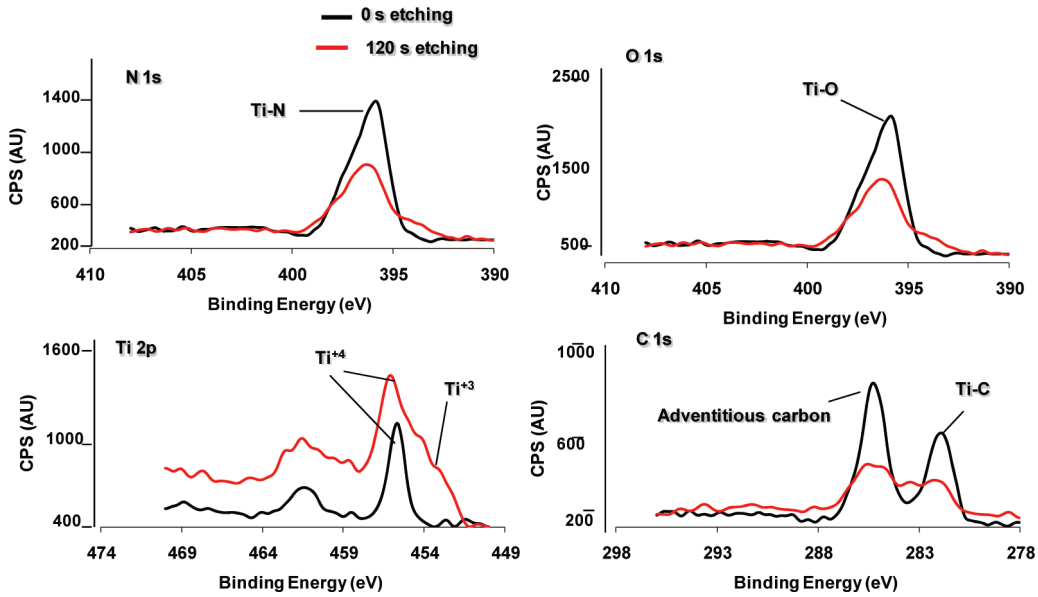

Figure 3. XPS Ar^+ sputtering measurements (etching time of 120 s) of D-TKP 102-B powder.

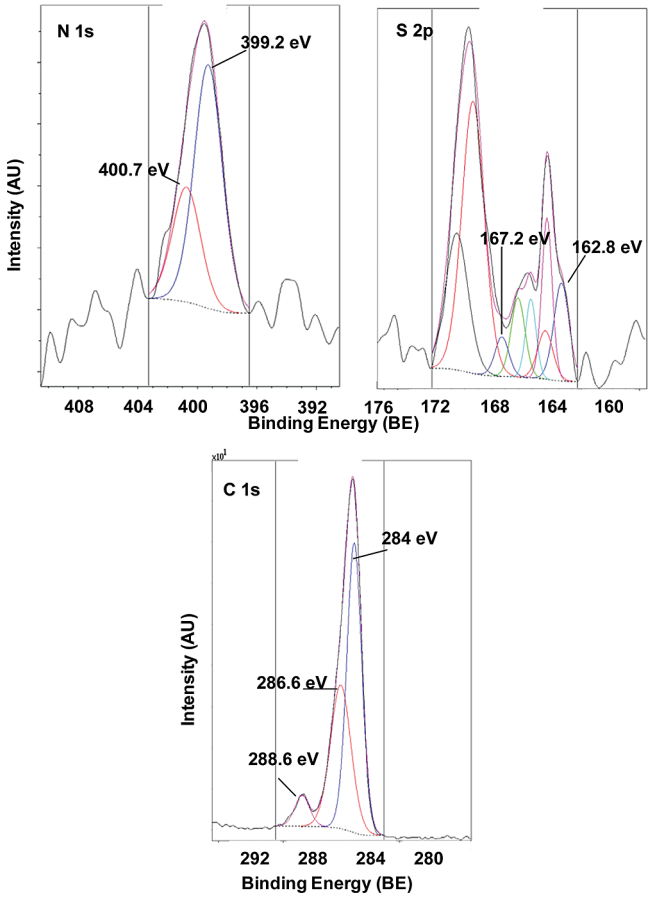

Figure 4. High-resolution XPS spectra of N 1s and S 2p peaks in D-TKP 102-A powder.

TABLE 1: N and S Content of D-TKP 102-A and D-TKP 102-B Measured by XPS

powder	N 1s (at. %)	S 2s (at. %)
doped TKP 102-A	0.54	0.71
doped TKP 102-B	37.48	0.85

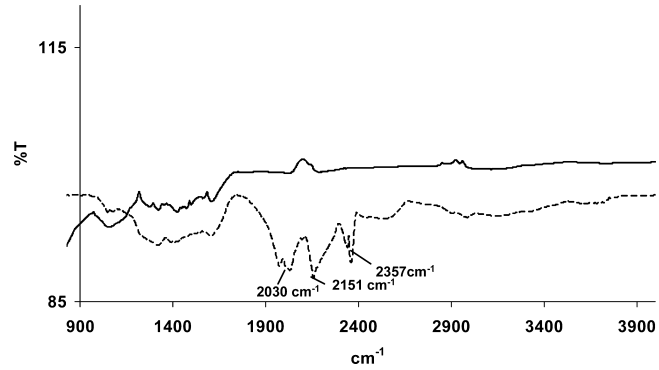

Figure 6. FTIR-ATR measurements of D-TKP 102-A and D-TKP 102-B powders.

etching time. However, different results were observed for the Ar^+-sputtered D-TKP 102-A sample. After 120 s of etching, the N 1s peak was shifted to BE 396 eV from the initial value of 399 eV. This results have already reported by Diwald et al.,[10] where a N 1s peak was detected at 399 eV on the TiO_2 surface and then, during the Ar^+ sputtering, a new peak at 396 eV commonly linked to Ti−N bonds formation appeared. These results might give evidence that in D-TKP 102-B the N and C species could be on the TiO_2 surface while in D-TKP 102-A N species could also be on the semiconductor bulk. However, Beranek and Kisch[30] have suggested that Ar^+ sputtering could produce modifications on the surface properties of the TiO_2. We detected the possible formation of Ti^{3+} species in XPS spectra of D-TKP 102-A and B probably induced by Ar^+ sputtering. Thus, it is not possible to conclude that in D-TKP 102-A the N-doping could also be on the semiconductor bulk.

3.3. Attenuated Total Reflectance IR Spectroscopy (ATR-FTIR). The ATR-FTIR spectra of annealed D-TKP 102-B and D-TKP 102-A powders are shown in the Figure 6. D-TKP 102-A did not reveal detectable IR signals, while the D-TKP102-B sample showed vibrational peaks between 2000 and 2300 cm^{-1} assigned to −NCS, −NCO, or −CN bands. However, Randeniya et al.[25] found IR signals at 2045 cm^{-1} for isothiocyanate or thiocyanate for S-doped samples of TiO_2 employing thiourea as doping precursor. In Figure 5 peaks at 2151−2357 cm^{-1}

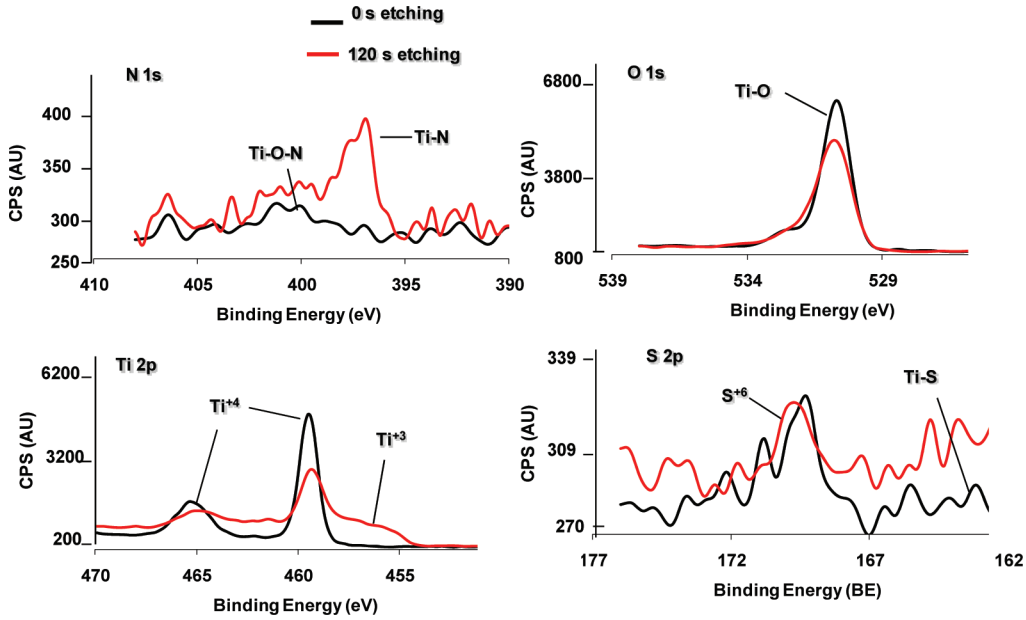

Figure 5. XPS Ar^+ sputtering measurements (etching time of 120 s) of D-TKP 102-A powder.

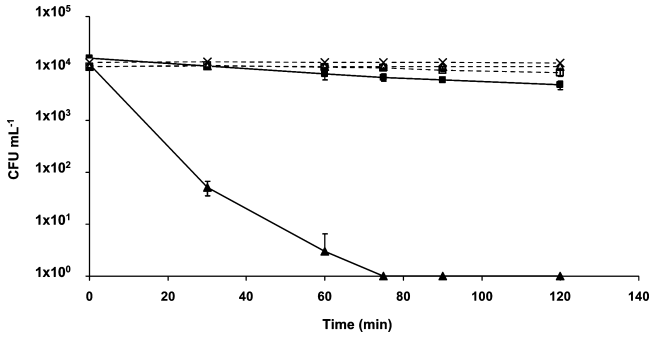

Figure 7. Photocatalytic *E. coli* inactivation under visible light exposition: (-■-) D-TKP 102-B, (-▲-) D-TKP 102-A, (---×---) only visible light, (---Δ---) D-TKP 102-A in the dark, and (---□---) D-TKP 102-B in the dark).

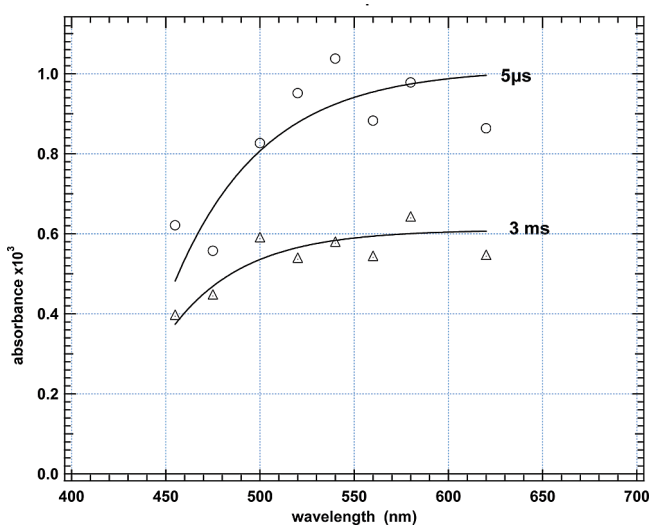

Figure 8. Transient absorption spectra of D-TKP 102-A powder.

could be due to bands of Ti-isothiocynate or thiocyanate complex.[31−33]

We suggest that Ti−N and Ti−C XPS signals found in D-TKP 102-B could be due to the presence of Ti-NCS and Ti-CN complexes on the titania surface inducing visible light absorption. Thus, D-TKP 102-B is not an N-doped TiO_2 material. As consequence, when the crucible *S*/*V* ratio was smaller, the oxygen content close to the TiO_2/thiourea mix was lowest and the thiourea was not efficiently oxidized leaving combustion byproduct in contact with the TiO_2 surface and leading finally to the possible formation of Ti-isothiocynate or thiocyanate complexes responsible for the visible light absorption.

3.4. Photocatalytic *E. coli* Inactivation under Visible Light. D-TKP 102-A and D-TKP 102-B powders did not inactivate *E. coli* in the dark. Photocatalytic *E. coli* inactivation was carried out using D-TKP 102-B and D-TKP 102-A powders as photocatalyst under visible light exposition (400−500 nm) as shown in Figure 7. It was observed that D-TKP 102-A mediated a higher photocatalytic *E. coli* inactivation than D-TKP 102-B. As it was mentioned in section 3.3, D-TKP 102-B reveals Ti-thiocyanate or Ti-isothiocyanate complexes formation on the TiO_2 surfaces. These N, C, or S species would induce visible light absorption but do not allow electron transfer on the catalyst surface under light acting as recombination centers. Section 3.5 below shows that the D-TKP 102-A sample had a high photocatalytic activity toward *E. coli* inactivation.

3.5. Mechanism of Photocatalytic *E. coli* Inactivation with D-TKP 102-A Powder. It is well-known that the first events occurring in photocatalytic reactions on TiO_2 are the generation

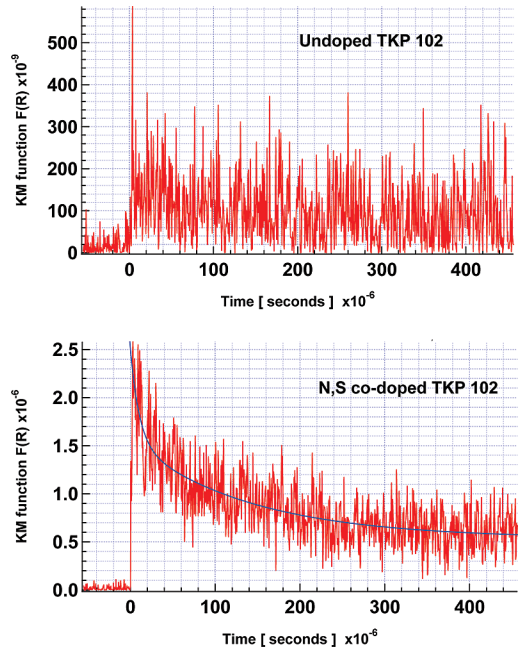

Figure 9. Signal of transient absorption of undoped TKP 102 and D-TKP 102-A powders.

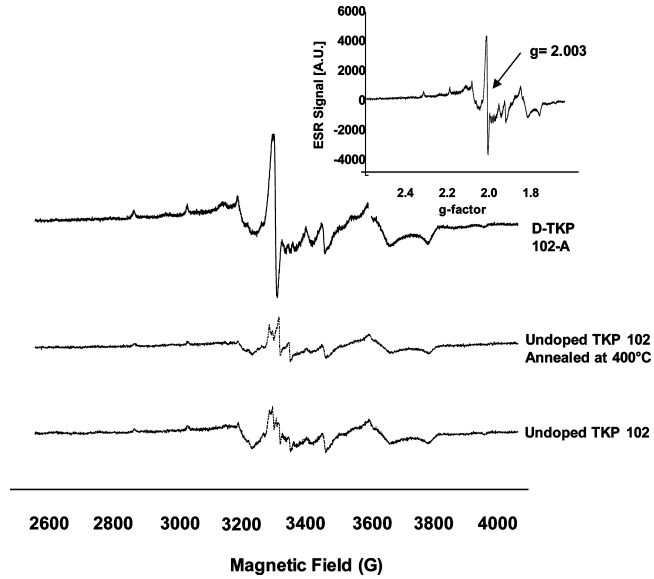

Figure 10. Low-temperature ESR spectra of undoped powder, undoped powder annealed at 400 °C, and D-TKP 102-A taken at 8 K. Inset shows the ESR signal Vs *g*-factor.

and separation of electron/hole pairs induced by light absorption. We used time-resolved diffuse reflectance spectroscopy (TRDR) and low-temperature electronic spin resonance (LT-ESR) to detect the electron promotion under visible light and the trapping features of the electron on D-TKP 102-A powders. The TRDR technique[34−37] has also been used to study the decay of the electron in TiO_2 powders.[38,39] The absorption of the electron was followed at 600 nm (ϵ_{600} = 1200 M^{-1} cm^{-1}).[32,33] The transient absorption spectrum in Figure 8 for D-TKP 102-A powder undergoing a laser pulse with λ = 450 nm showed the existence of a maximum around 550 nm after 5 s of laser pulse and extending to the limit of the oscilloscope of 2 ms due to electron trapping on TiO_2 dehydrated shallow traps.[34]

The signal of transient absorption upon visible laser pulse in Figure 9 shows that the undoped TKP 102 powder did not reveal any signal while D-TKP 102-A showed the signal for electrons

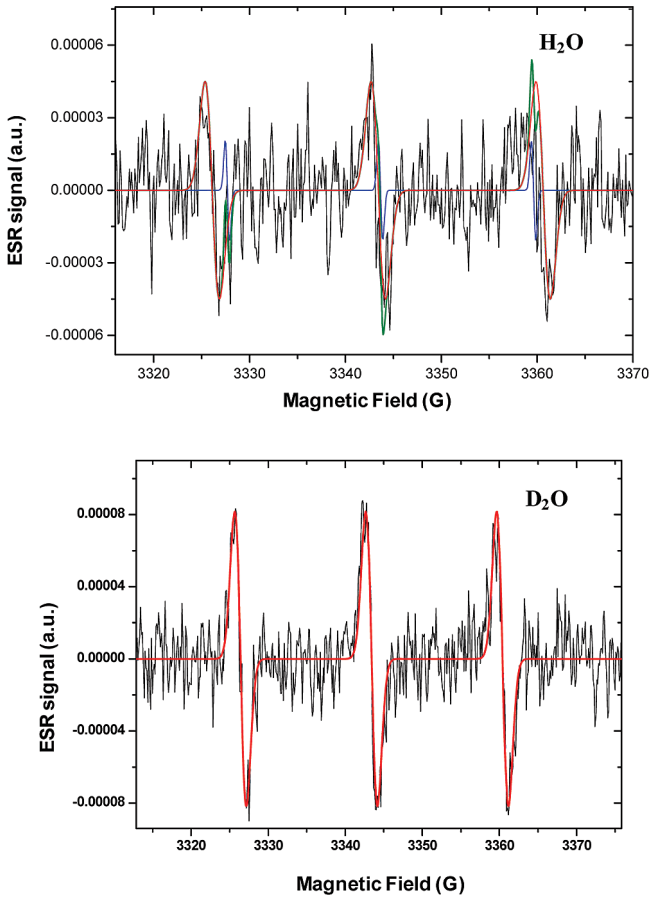

Figure 11. ESR spectra of TEMPOL observed after 16 min of illumination with visible light of the aqueous suspensions of N, S-codoped nano-TiO_2 in the presence of 2.5 mM concentration of singlet oxygen scavenger, TMP−OH. Upper panel: ESR trace recorded in H_2O. Lower panel: ESR trace recorded in D_2O. Red solid line corresponds to a simulative fit of the ESR spectrum of TEMPOL (A_{iso} = 17.4 G).

on TiO_2, with two components: a faster one due to the electron decay and a long-lived component with 1/4 of the initial amplitude due to the electron trapping on shallow TiO_2 traps. It is often is assumed that photoexcited electrons in TiO_2 are trapped on Ti^{IV} sites or oxygen vacancies V_o, and it is believed that molecular oxygen is adsorbed on the same sites.[2,40,42]

By means of LT-ESR, we investigated the presence of V_o in undoped TiO_2 and D-TKP 102-A powders (Figure 10). A signal with g = 2.0030 was found for the powder D-TKP-102-A. This signal has often been assigned to a single electron trapped in an oxygen vacancy (V_o).[40−45] Annealing of undoped powders was unable to generate V_o. Livraghi et al. recently demonstrated that N-doping of TiO_2 could induced the formation of oxygen vacancies.[15] Emeline et al.[4] have reported that N-doping stabilizes the oxygen vacancies by defect charge compensation. We did not find NO ESR signals for NO species adsorbed on N-doped TiO_2 as reported by Di Valentin.[46] It is well-known that oxygen vacancies participate in photocatalytic reactions as electron traps, charge transfer sites, and adsorption sites of molecular oxygen.[2,41]

We also performed ESR spin trapping experiments using TMP−OH as singlet oxygen indicator. Singlet oxygen was identified by the characteristic 1:1:1 triplet signal of TEMPOL (Figure 11). Moreover, in the presence of singlet oxygen the ESR signal of TEMPOL was markedly enhanced when using D_2O as solvent.[47,48] Konaka et al.[49] reported a similar isotopic enhancement of the ESR signal of singlet in TiO_2−D_2O suspensions. Recently we found that the •OH radical is not produced under visible light in the presence of N, S-codoped TKP 102 TiO_2[21]. Furthermore, recently it has been suggested[13,14,50] that the hydroxyl radicals were not formed on the illuminated N-, S-, or C-doped TiO_2 nanoparticles since the photoinduced holes on the midgap levels do not reach the redox potential necessary to induce these radicals. Hirakawa and Nosaka[50] found that photoexcited electrons led to superoxide radicals/H_2O_2 responsible for the photoactivity of the N- and S-doped TiO_2 powders.

Finally, we suggest that the N, S-TKP 102-A powders could excite electrons from midgap levels to the conduction band by visible light absorption. These electrons could react with the molecular oxygen previously adsorbed on oxygen vacancies (EPR signal with g = 2.003) producing superoxide radicals. This later radical may be oxidized by the holes trapped on the midgap N, S states leading to singlet oxygen inactivating *E. coli* (Scheme 1).

4. Conclusions

In this work, we successfully synthesized a visible-light-harvesting photocatalyst, N, S-codoped TiO_2, by reacting thiourea with nanoparticulate commercial anatase TiO_2. Thiourea and anatase were manually ground and annealed at 400 °C.

The differentiated aeration conditions during the catalyst annealing by using two crucibles having different *S*/*V* ratios

SCHEME 1: Mechanism of Singlet Oxygen Formation on D-TKP-102-A Surfaces[a]

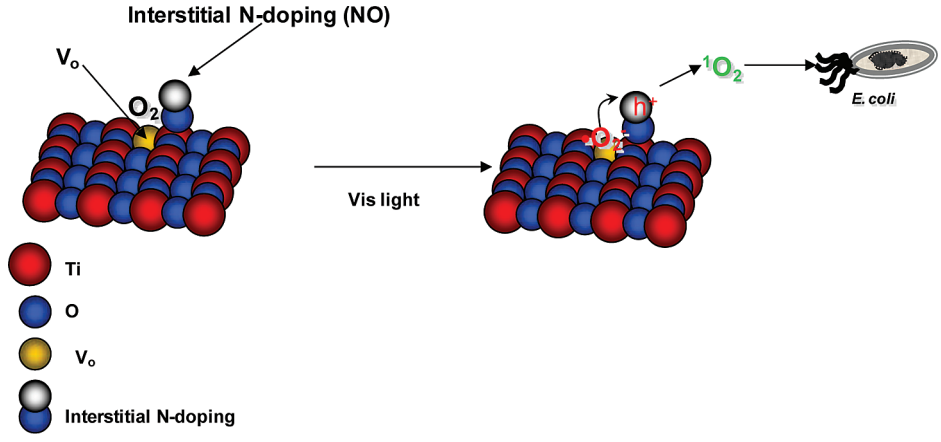

[a] Gray circles = Ti, black = oxygen.

allowed for different amounts of O_2 to reach the catalyst surface, thus resulting in two TiO_2 materials absorbing visible light.

D-TKP 102-B ($S/V = 1.5$) powder showed higher visible light absorption but much lower activity toward *E. coli* inactivation probably due to the presence of higher N and C contents (revealed by XPS measurements). FTIR results showed evidence of the formation of Ti−NCS or Ti−CN complexes on the powder surface acting as recombination centers.

The *E. coli* inactivation under visible light seems to be due to the electronic promotion from N, S-localized states within the band gap induced by the N, S-codoping as shown by DRTRS experiments. The D-TKP 102-A ($S/V = 20$) powder promotes electrons from N, S states within the band gap to the conduction band by visible light exposition leaving a localized hole in the valence band. LT-ESR measurements revealed that the formation of oxygen vacancies was enhanced by N, S-codoping.

The formation of singlet oxygen ($^1O_2$) on D-TKP 102-A samples activated by visible light is suggested during *E. coli* inactivation.

Acknowledgment. The authors thank the Swiss Agency for Development and Cooperation and Cooperation@EPFL for its support of the BIOSOLARDETOX project, J. Teuscher from the Photochemical Dynamics Group (EPFL−Switzerland) for help in the recording of DRS spectra, and O. Masaaki from Tayca Corp (Japan) and S. Jansen from Mitsubishi Corp (Germany) for kindly supplying the samples of TiO_2 powders Tayca. These studies were also partially supported by the Swiss National Science Foundation, project No. 205320-112164, "Biomolecules under stress: ESR in vitro study" (A.S., K.P., and L.F.). We also thank COST Action 540 PHONASUM for financial support.

References and Notes

(1) Hoffmann, M. R.; Martin, S. T.; Choi, W.; Bahnemann, D. W. *Chem. Rev.* **1995**, *95*, 69–69.
(2) Thompson, T. L.; Yates, J. T. *Chem. Rev.* **2006**, *106*, 4428–44.
(3) Hashimoto, K.; Irie, H.; Fujishima, A. *Jpn. J. Appl. Phys.* **2005**, *44*, 8269–8285.
(4) Emeline, A. V.; Kuznetsov, V. N.; Rybchuk, V. K.; Serpone, N. *Int. J. Photoenergy* **2008**, *2008*, 19; article ID 258394,, doi: 10.1155/2008/258394.
(5) Choi, W. Y.; Termin, A.; Hoffmann, M. R. *Angew. Chem.* **1994**, *106*, 1148–1149.
(6) Burda, C.; Lou, Y. B.; Chen, X. B.; Samia, A. C. S.; Stout, J.; Gole, J. L. *Nano Lett.* **2003**, *3*, 1049–1051.
(7) Asahi, R.; Morikawa, T.; Ohwaki, T.; Aoki, K.; Taga, Y. *Science* **2001**, *293*, 269–271.
(8) Nambu, A.; Graciani, J.; Rodriguez, J. A.; Wu, Q.; Fujita, E.; Fernandez-Sanz, J. J. *Chem. Phys.* **2006**, *125*, 094706-1−094706-8.
(9) Diwald, O.; Thompson, T. L.; Goralski, E. G.; Walck, S. D.; Yates, J. T. *J. Phys. Chem. B* **2004**, *108*, 52–57.
(10) Diwald, O.; Thompson, T. L.; Zubkov, T.; Goralski, E. G.; Walck, S. D.; Yates, J. T. *J. Phys. Chem. B* **2004**, *108*, 6004–6008.
(11) Livraghi, S.; Chierotti, M. R.; Giamello, E.; Magnacca, G.; Paganini, M. C.; Cappelletti, G.; Bianchi, C. L. *J. Phys. Chem. C* **2008**, *112*, 17244–17252.
(12) Fu, H.; Zhang, L.; Zhu, Y.; Zhao, J. *J. Phys. Chem. B* **2006**, *110*, 3061–3065.
(13) Mrowetz, M.; Balcerski, W.; Colussi, A. J.; Hoffmann, M. R. *J. Phys. Chem. B* **2004**, *108*, 17269–17263.
(14) Tachikawa, T.; Tojo, S.; Kawai, K.; Endo, M.; Fujitsuka, M.; Ohno, T.; Nishijima, K.; Miyamoto, Z.; Majima, T. *J. Phys. Chem. B* **2004**, *108*, 19299–19306.
(15) Livraghi, S.; Paganini, M. C.; Giamello, E.; Selloni, A.; Di Valentin, C.; Pacchioni, G. *J. Am. Chem. Soc.* **2006**, *128*, 15666–15671.
(16) Rengifo-Herrera, J. A.; Pierzchala, K.; Sienkiewicz, A.; Forró, L.; Kiwi, J.; Pulgarin, C. *Appl. Catal., B*; doi: 10.1016/j.apcatb.200.10.025.
(17) Lion, Y.; Delmelle, M.; Van de Vorst, A. *Nature* **1976**, *263*, 442–443.
(18) Ando, T.; Yoshikawa, T.; Tanigawa, T.; Kohno, M.; Yoshida, N.; Kondo, M. *Life Sci.* **1997**, *61*, 1953–1959.
(19) Diwald, O.; Thompson, T. L.; Goralski, E. G.; Walck, S. D.; Yates, J. T. *J. Phys. Chem. B.* **2004**, *108*, 52–57.
(20) Saha, N. C.; Tompkins, H. G. *J. Appl. Phys.* **1992**, *72*, 3072–3079.
(21) Chen, X.; Lou, Y.; Samia, A. C.; Burda, C.; Gole, J. L. *Adv. Funct. Mater.* **2005**, *15*, 41–49.
(22) Sun, H.; Bai, Y.; Cheng, Y.; Jin, W.; Xu, N. *Ind. Eng. Chem. Res.* **2006**, *45*, 4971–4976.
(23) Liu, S.; Chen, X. *J. Hazard. Mater.* **2008**, *152*, 48–55.
(24) Zhang, L.; Koka, R. V. *Mater. Chem. Phys.* **1998**, *57*, 23–32.
(25) Randeniya, L. K.; Murphy, A. B.; Plumb, I. C. *J. Mater. Sci.* **2008**, *43*, 1389–1399.
(26) Ohno, T.; Akiyoshi, M.; Umebayashi, T.; Asai, K.; Mitsui, T.; Matsamura, M. *Appl. Catal., A* **2004**, *265*, 115–121.
(27) Umebayashi, T.; Yamaki, T.; Itoh, H.; Asai, K. *Appl. Phys. Lett.* **2002**, *81*, 454–456.
(28) Beranek, R.; Kisch, H. *Photochem. Photobiol. Sci.* **2008**, *7*, 40–48.
(29) Goodall, D. C. *J. Chem. Soc. A* **1967**, 203–204.
(30) Mitchell, P.C. H.; Williams, R. J. P. *J. Chem. Soc.* **1960**, 1912.
(31) Frank, R.; Droll, H. A. *J. Inorg. Nucl. Chem.* **1970**, *32*, 3954–3956.
(32) Colombo, D. P.; Bowman, R. M. *J. Phys. Chem.* **1996**, *100*, 18445–18449.
(33) Rothemberger, G.; Moser, J.; Gratzel, M.; Serpone, N.; Sharma, D. K. *J. Am. Chem. Soc.* **1985**, *107*, 8054–8059.
(34) Moser, J. Ph.D. Dissertation, Thesis No. 616, Ecole Polytechnique Fédérale de Lausanne, Lausanne, Switzerland, 1986.
(35) Serpone, N.; Lawless, D.; Khairutdinov, R.; Pelizzetti, E. *J. Phys. Chem.* **1995**, *99*, 16655–16661.
(36) Kim, S.; Choi, W. *J. Phys. Chem. B* **2005**, *109*, 5143–5149.
(37) Draper, R. B.; Fox, M. A. *Langmuir* **1990**, *6*, 1396–1402.
(38) Colombo, D. P.; Bowman, R. M. *J. Phys. Chem.* **1996**, *100*, 18445–18449.
(39) Colombo, D. P.; Bowman, R. M. *J. Phys. Chem.* **1995**, *99*, 11752–11756.
(40) Naccache, C.; Meriaudeau, P.; Che, M. *Trans. Faraday Soc.* **1971**, *67*, 506–512.
(41) Green, J.; Carter, E.; Murphy, D. M. *Chem. Phys. Lett.* **2009**, *477*, 340–344.
(42) Serwicka, E.; Schlierkamp, M. W.; Schindler, R. N. *Z. Naturforsch.* **1981**, *36a*, 226–232.
(43) Sun, Y.; Egawa, T.; Shao, C.; Zhang, L.; Yao, X. *J. Cryst. Growth* **2004**, 118–122.
(44) Feng, C.; Wang, Y.; Jin, Z.; Zhang, J.; Zhang, Z.; Wu, Z.; Zhang, Z. *New J. Chem.* **2008**, *32*, 1038–1047.
(45) Kuznetsov, V. N.; Serpone, N. *J. Phys Chem. C* **2009**, *113*, 15110–15123.
(46) Di Valentin, C.; Finazzi, E.; Pacchioni, G.; Selloni, A.; Livraghi, S.; Paganini, M. C.; Giamello, E. *Chem. Phys.* **2007**, *339*, 44–56.
(47) Vileno, B.; Lekka, M.; Sienkiewicz, A.; Marcoux, P.; Kulik, A. J.; Kasas, S.; Catsicas, S.; Gaczyk, A.; Forró, L. *J. Phys.: Condens. Matter* **2005**, *17*, S1471–S1482.
(48) Andersen, L. K.; Ogilby, P. R. *J. Phys. Chem. A.* **2002**, *106*, 11064–11069.
(49) Konaka, R.; Kasahara, E.; Dunlap, W. C.; Yamamoto, Y.; Cheng-Chien, K.; Inoue, M. *Redox Rep.* **2001**, *6*, 319–325.
(50) Hirakawa, T.; Nosaka, Y. *J. Phys. Chem. C* **2008**, *112*, 15818–15823.

JP910486F